PCCP

ROYAL SOCIETY OF CHEMISTRY

PAPER

View Article Online
View Journal



Cite this: DOI: 10.1039/d5cp03418c

# Associative *vs.* dissociative binding of $CO_2$ on $M_5$ transition metal clusters

Nguyen T. T. Le, Alireza Nazari, Yash Rele, Mighila Rixon, Ishudeep Singh Narula and Matthew A. Addicoat *

Received 4th September 2025,
Accepted 8th December 2025

DOI: 10.1039/d5cp03418c

rsc.li/pccp

Reaction paths were calculated using density functional theory for the reaction of carbon dioxide with a series of transition metal pentamers, $M_5$ + $CO_2$, (M = Nb, Mo, Ru, Rh, Pd, Ag, Pt). A stochastic search algorithm was used to identify geometries with intact $CO_2$, as well as geometries where the $CO_2$ molecule was partly (O + CO) and fully dissociated (O + C + O). $Nb_5$ and $Mo_5$ clusters were found to thermodynamically dissociate $CO_2$. $Pd_5$ and $Ag_5$ were found to leave the $CO_2$ molecule intact, $Ru_5$ could partly dissociate $CO_2$, while for $Rh_5$ and $Pt_5$, the fate of the adsorbed $CO_2$ was dependent on the cluster geometry. The change in the $CO_2$ $\pi_u$ orbital energy in the capture species on initial reaction with the $M_5$ cluster was found to distinguish clusters where $CO_2$ fully dissociated, but could not distinguish clusters where $CO_2$ was found to partly dissociate. The charge transfer to the $CO_2$ molecule at the first transition state, did however, distinguish clusters that fully dissociate $CO_2$, those that partly dissociate $CO_2$ to O + CO, and those that leave $CO_2$ fully intact.



## 1. Introduction

In recent years, there has been increasing interest in the activation of $CO_2$. Especially in the context of the environment, the ability to activate captured $CO_2$ towards further reaction, turns a problem of needing to store the captured $CO_2$[1] into a solution – a cheap C1 feedstock.[2,3] $CO_2$ is unfortunately well-known for its thermodynamic and kinetic stability, and it is unreactive in the gas phase,[4] thus requiring activation *via* some catalyst species in order to weaken and/or break the CO bonds. Activation of $CO_2$ typically proceeds *via* introducing electron density into the antibonding $\pi^*$ orbitals of $CO_2$, weakening the C═O bonds and allowing the $CO_2$ the molecule to bend away from linear, simultaneously creating a dipole and increasing the reactivity of $CO_2$.[5–7]

Several manufactured materials including foams,[8] $CaCO_3$ microspheres,[9] and novel cements[10] have been proposed and used to capture and store $CO_2$. More recently, novel materials including, Metal- and Covalent Organic Frameworks,[11–13] carbon nanotubes,[14] MXenes,[15–20] and nanofilms[21] have been proposed to not only capture, but to valorize $CO_2$ for further use. $CO_2$ is activated by electron donation into the antibonding $\pi^*$ orbitals of $CO_2$, weakening the C═O bonds allowing the $CO_2$ molecule to bend.[5–7,22,23] In the majority of these materials above, the active site of the catalyst is a metal atom[24] and thus there is considerable interest in the mechanism of $CO_2$ activation by various metals[25] and there has been a great volume of spectroscopic and theoretical work over decades[26–29] investigating the interaction of $CO_2$ with single transition metal atoms/ions, $M^{+/0/-}$. A range of $CO_2$ binding motifs have thus been identified, including $\eta^1$ coordination (*via* the C atom), bidentate $\eta^2$ binding (*via* C, O), and dissociative addition where binding produces CO and O species. Where multiple $CO_2$ molecules adsorb, oxalate formation has also been identified.[7,30]

In between single atoms and bulk surfaces, transition metal clusters have long been an avenue for the investigation of gas phase reactions, with a variety of substrates including CO,[22,31] $N_2O$[32] and notably $CO_2$.[32,34,35] Size effects are well-known in the cluster regime, with several experimental[36] and computational studies[37] noting properties varying over several orders of magnitude upon single atom addition.

One study from Mackenzie group illustrated these size effects with respect to $CO_2$ activation, employing small $Pt_4^-$ and $Pt_5^-$ anionic clusters. They showed that while $Pt_4^-$ + $CO_2$ has a dissociative global minimum (*i.e.* $Pt_4^-$(CO)O), the spectroscopically observed species possessed intact $CO_2$ ($Pt_4^-$OCO), whereas for the one atom larger cluster anion, $Pt_5^-$, infrared multiphoton dissociation (IR-MPD) spectroscopy showed the computationally predicted global minimum, dissociatively bound $Pt_5^-$(CO)O exists and in contrast to $Pt_4^-$, no evidence of molecularly bound $CO_2$ was seen, despite such a species being predicted within the energy of their cluster source.[38]

Inspired by this work of Mackenzie *et al.*,[38] and following on from our work on $M_4$ clusters,[39] we report a ''horizontal'' study, investigating the reaction of $CO_2$ with $M_5$ neutral transition metal clusters from niobium through silver and additionally including platinum.

*School of Science and Technology, Nottingham Trent University, Clifton Lane, Nottingham, NG11 8NS, UK. E-mail: matthew.addicoat@ntu.ac.uk*

## 2. Computational method

The computational method employed here is the same as in our previous work, and recapped here.[39] Structures of $M_5$ clusters, for M = Nb–Ag (excluding Tc) and Pt were generated using the Kick stochastic structure search procedure with five individual M atoms supplied.[40,41] Full searches were undertaken on the lowest possible multiplicity (singlet or doublet) and all minima identified were re-optimized at higher multiplicities. For all metal species, the lowest four multiplicities were calculated, but for ruthenium and rhodium, the search was extended up to the 15-tet and the 12-tet, respectively. No symmetry was imposed at any point in the search, nevertheless, several clusters adopted clear point group symmetry, as evidenced by geometric parameters and frequencies. We chose not to confirm the symmetry by further calculation, as the addition of $CO_2$ would immediately break symmetry.

The lowest energy structure of each $M_5$ cluster was then adopted as a fragment in a further stochastic search process. Kick runs were undertaken with the following configurations: $M_5 + CO_2$(linear); $M_5 + CO_2$(bent); $M_5 + CO + O$; $M_5 + C + O + O$. In order to easily identify the transition state where the $CO_2$ molecule first began to dissociate, a Kick run was also undertaken explicitly searching for transition states, employing the $M_5$ cluster and the bent $CO_2$ molecule as fragments. Additional starting geometries were generated by hand (*e.g.* $CO_2$ bound to different symmetry-distinct metal atoms, end-on/side-on, linear/bent, $\mu^1/\mu^2/\mu^3$-bound). From these calculations, the physisorbed ''capture'' species and the $M_5CO_2$ global minimum were identified, and the reaction pathway was then filled in and confirmed by a series of Quasi-Synchronous Transit (QST) and Intrinsic Reaction Coordinate (IRC) calculations.

The zero energy for each $M_5 + CO_2$ system is defined as the sum of the energies of the $M_5$ metal cluster in the lowest possible multiplicity and the $CO_2$ molecule. Thus structures with a negative relative energy (below the zero energy) are more stable than the separated reactants; structures with a positive relative energy (energy higher than the zero energy) are unstable with respect to the infinitely separated reactants. basis set superposition error (BSSE) was disregarded, as were zero-point energies and entropic contributions, as previous work that the effect of BSSE and ZPE on relative energies is minimal and that adding entropic effects was found to consistently raise relative energies by $\approx$0.5 eV at 298 K.[31] All structure searches were undertaken with the B3P86 density functional[42] and Stuttgart Relativistic Small Core (SRSC) basis set,[43–45] as previous studies[31,46] have shown this to be an accurate and computationally efficient combination. The final pathways were re-optimized at all relevant multiplicities using the TPSS functional[47] with the Def2TZVP basis set[48,49] and employing the D3-BJ empirical dispersion term.[50] This latter combination, while more expensive, has also been shown to reproduce energetic ordering and vibrational data for reactions of small molecules on gas phase transition metal clusters including $Rh_n$[51] and $Pt_n$.[52] All calculations were undertaken using the Gaussian 16 software.[53] All structures presented are included in the SI (xyz, zip) and absolute and relative energies for each structure at all multiplicities studied are presented in the SI (xlsx).

## 3. Results and discussion

### 3.1. $Nb_5$

The $Nb_5$ cluster is an odd-electron species and therefore may be a doublet, quartet,.... The doublet multiplicity was found to be the lowest in energy, in line with previous calculations.[54] In slight contrast to the early calculations of Salahub *et al.* on neutral $Nb_5$, we identified the minimum energy structure to be of $C_{2v}$ symmetry with equatorial–equatorial bond lengths of 2.63 (2) and 2.87 Å and axial–equatorial bond lengths of 2.49 (2) and 2.61 Å. This cluster was used for the $CO_2$ pathway without constraint.

Two pathways were identified for the reaction of $Nb_5 + CO_2$, shown in Fig. 1 and 2. Corresponding geometric data is shown in Table S1. Both pathways begin with the $CO_2$ molecule approaching the equatorial niobium atoms, and the $CO_2$ molecule bending over one of the triangular faces of the $Nb_5$ cluster. Structures *I–V* of both pathways are therefore the same. The two pathways diverge with a choice of which CO bond breaks first. In the pathway shown in Fig. 1, the CO bond that is closest to the equatorial plane of the $Nb_5$ cluster breaks first resulting in a CO molecule bound to an axial niobium atom and the lone oxygen atom attached to an equatorial niobium atom. The second pathway, shown in Fig. 2 breaks the other CO bond, resulting in the CO molecule bound to equatorial niobium atoms and the dissociated oxygen atom bound to an axial niobium atom. Both pathways result in very similar global minima, with the $CO_2$ molecule completely dissociated, at relative energies of −6.76 and −6.68 eV respectively. These two structures, Fig. 1-IX and 2-XI, may interconvert, *via* a transition state shown on the first pathway, Fig. 1-X.

### 3.2. $Mo_5$

The molybdenum atom is and even-electron species and therefore the $Mo_5$ cluster is also an even-electron species and we investigate the singlet, triplet,... surfaces. Several authors have calculated the structure and properties of the $Mo_5$ cluster using a variety of density functional methods, basis sets and structure search approaches. Plá and Diez identified a singlet global minimum of a capped out-of-plane rhombus, but with singlet and triplet trigonal bipyramid structures both only 0.03 eV per atom higher in energy.[55] Vega and coworkers predicted a triplet bipyramid with $C_{2v}$ symmetry,[56] while Yin and Chen identified a singlet trigonal bipyramid with $C_1$ symmetry.[57] Kantorovich and coworkers used the AIRSS approach[58] to identify 9 $Mo_5$ structures within 1 eV of the global minimum, which they predict to be a $C_{2v}$ singlet trigonal bipyramid.[59] Sumer and Jellinek identified a similar set of low energy structures, but their global minimum had only $C_2$ symmetry.[60] Lei predicted a singlet trigonal bipyramid structure.[61] In general agreement with these studies, we identified the global minimum to be a

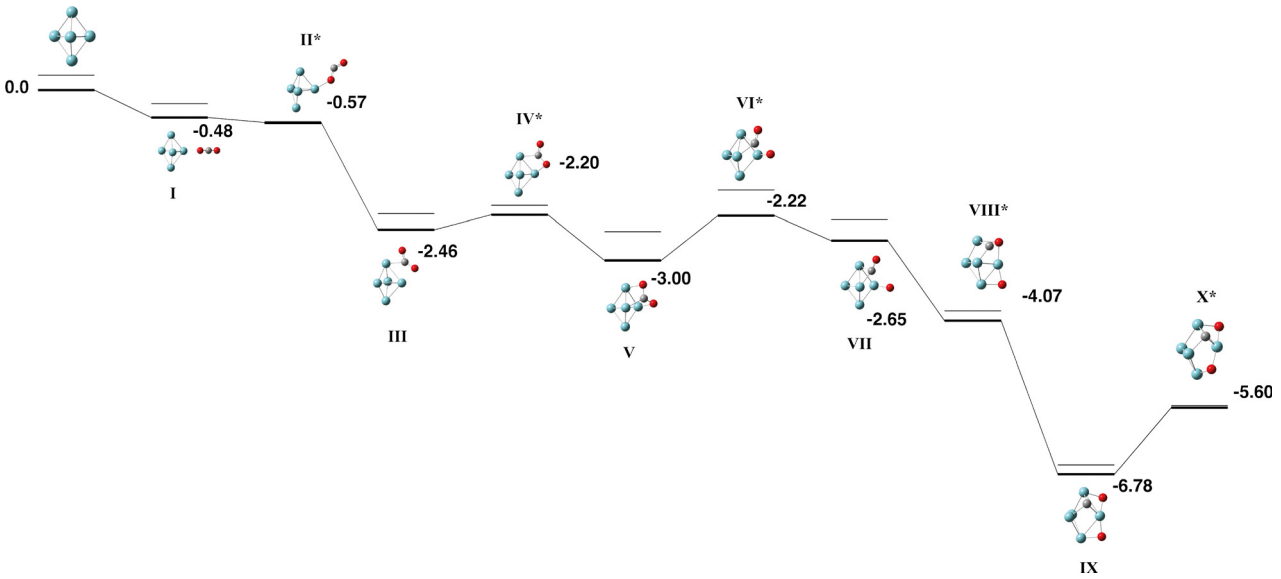


Fig. 1 Stationary points on the $Nb_5$ + $CO_2$ potential energy surface. The doublet multiplicity is shown in bold and the quartet multiplicity is shown with thin lines. Relative energies are given in eV. Metal atoms are shown in blue/green, oxygen atoms are shown in red and the carbon atom is shown in grey.

singlet trigonal bipyramid with approximately $D_{3h}$ symmetry and bond lengths of 2.34 Å (axial–equatorial) and 2.83 Å (equatorial–equatorial) and we employed this structure, without symmetry constraint, in our reaction with $CO_2$.

A single pathway was identified for the reaction of $Mo_5$ + $CO_2$, it is shown in Fig. 3 and Table S2. The pathway begins with the $CO_2$ molecule approaching the axial molybdenum atoms, and the $CO_2$ molecule breaks over the axial atom of the $Mo_5$ cluster in the first transition state (structure Fig. 3-II). The remaining CO molecule binds in a $\mu^3$ fashion to a triangular face of the $Mo_5$ cluster, before twisting, rotating parallel to the face and then dissociating. The $Mo_5CO_2$ global minimum therefore has the $CO_2$ molecule fully dissociated with the carbon atom $\mu^3$-bound, and the oxygen atoms $\mu^2$ and $\mu^1$-bound, with a relative binding energy of −4.91 eV with respect to the singlet $Mo_5$ + $CO_2$.

### 3.3. $Ru_5$

Ruthenium also has an even number of electrons and therefore we consider the singlet, triplet, quintet and septet multiplicities for the $Ru_5$ cluster. The $Ru_5$ cluster has been calculated previously by different authors and DFT methods,[62–65] but there is good agreement amongst researchers that the ground state structure of $Ru_5$ is a square pyramid structure with singlet multiplicity. We similarly identify a square pyramidal singlet

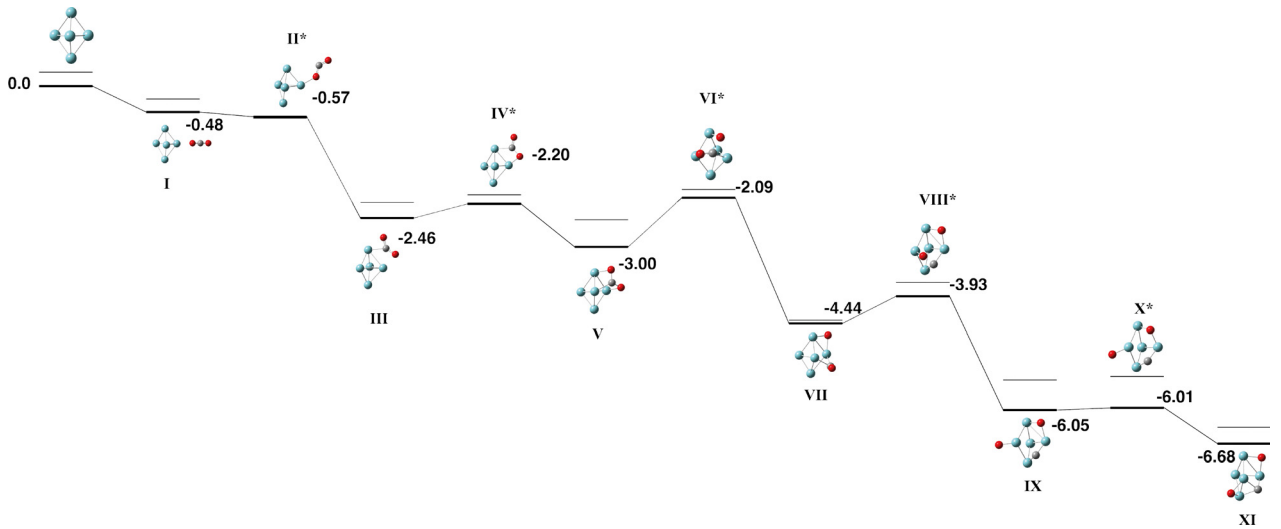


Fig. 2 Second reaction pathway on the $Nb_5$ + $CO_2$ potential energy surface. The doublet multiplicity is shown in bold and the quartet and sextet multiplicities are shown with thin lines. Relative energies are given in eV. Metal atoms are shown in blue/green, oxygen atoms are shown in red and the carbon atom is shown in grey.

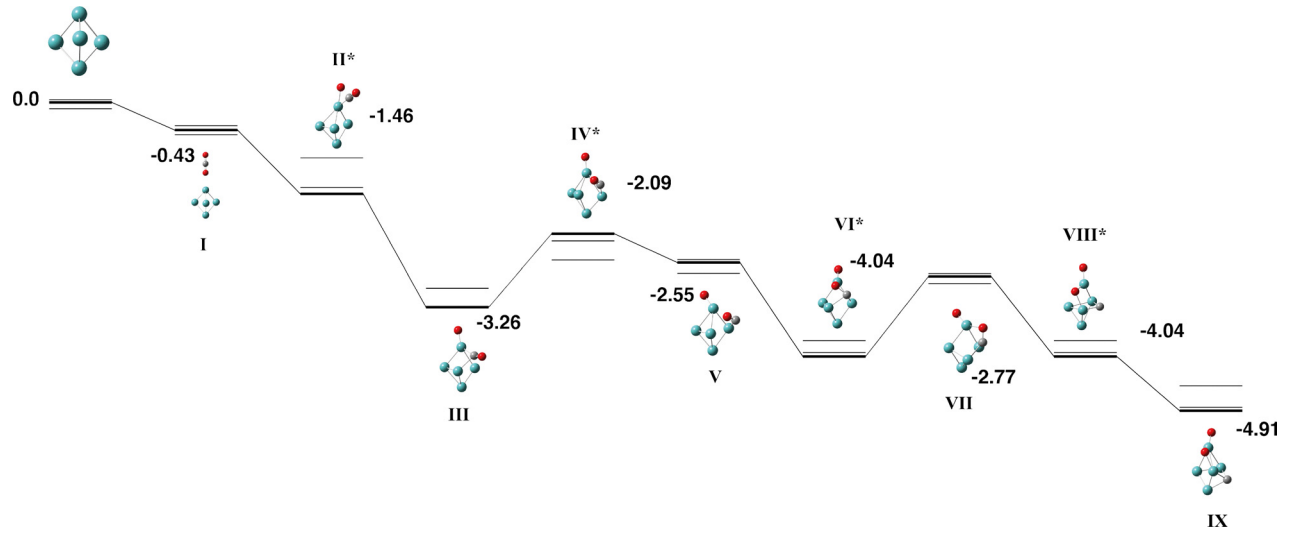


Fig. 3 Reaction pathway of $Mo_5 + CO_2$. The singlet potential energy surface is shown in bold and the triplet and quintet multiplicities are shown with thin lines. Relative energies for the singlet surface are given in eV, energies of higher multiplicities are included in SI (xlsx). Metal atoms are shown in blue/green, oxygen atoms are shown in red and the carbon atom is shown in grey.

structure with bond distances of 2.28 and 2.49 Å for the base–base and base–apex bonds respectively.

Two pathways were identified for the $Ru_5 + CO_2$ reaction, they are shown in Fig. 4 and 5. Corresponding geometric data is shown in Table S3. The singlet to nonet multiplicities were quite close in energy and so the pathway calculations were extended up to the 15-tet. The $CO_2$ molecule may approach either the apex ruthenium atom (Fig. 4) or one of the base ruthenium atoms (Fig. 5). In both cases, the first CO bond breaks with a barrier below the zero energy defined by $E[Ru_5(\text{singlet})] + E[CO_2]$, and leaving the CO molecule bound to the apex ruthenium atom. Two candidates for the global minimum $Ru_5CO_2$ structure are identified: The first structure has the CO molecule bound in a $\mu^1$ geometry to the apex Ru atom and the dissociated oxygen atom $\mu^1$-bound to a base Ru atom and in the $Ru_4$ plane. The second geometry has the CO molecule $\mu^2$-bound to the Ru(apex)–Ru(base) bond opposite the $\mu^1$-bound oxygen atom. These two geometries are interconvertible by a transition state at −2.15 eV (*i.e.* a 0.49 eV barrier) with an imaginary frequency of $134i$ $cm^{-1}$. The barrier to dissociating the second CO bond is 0.27 eV above zero energy for the singlet pathway, but below zero energy for the triplet to the 13-tet multiplicities. The lowest energy structure identified with $CO_2$ completely dissociated has a $\mu^1$ and a $\mu^2$ oxygen atom and a $\mu^2$-bound carbon atom. This structure has an energy of −2.17 eV, 0.47 eV higher in energy than the $Ru_5OCO$ global minima.

### 3.4. $Rh_5$

The $Rh_5$ cluster is an odd-electron species and therefore we consider the doublet – 12-tet multiplicities. Rhodium is of intense interest as a catalyst and many researchers have calculated the $Rh_5$ cluster. In an early study, Kelin and co-workers chose to model a trigonal bipyramid $Rh_5$, but did not investigate other geometries due to computational expense.[66] Rubio-Arroyo and coworkers predicted a twisted bowtie structure and two trigonal bipyramidal strucutres.[67] Aguilera-Granja *et al.* predict a square pyramidal $Rh_5$ cluster.[62] Futschek *et al.* predict three $Rh_5$ isomers, a $C_{4v}$ square pyramid and both a "tall" and a "flat" trigonal bipyramid structure, both of $D_{3h}$ symmetry.[68] Similarly, Pederson and coworkers present a sextet square pyramid as the ground state, with a trigonal bipyramid being

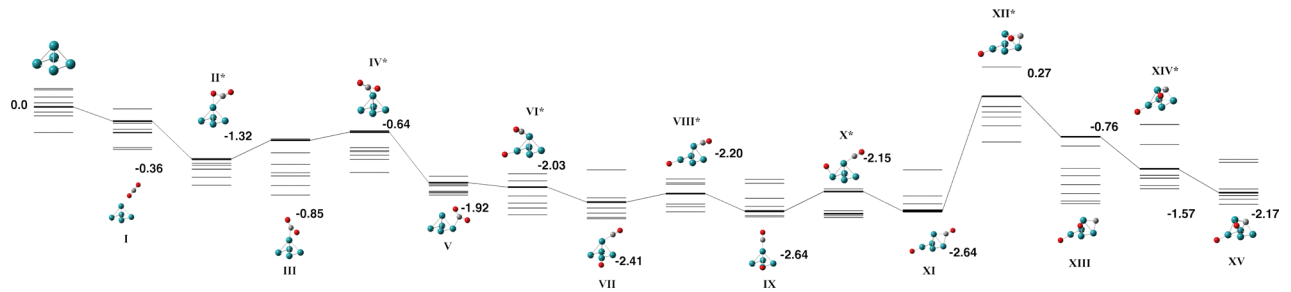


Fig. 4 Stationary points on the $Ru_5 + CO_2$ reaction pathway. The singlet potential energy surface is bolded and the triplet - 15-tet multiplicities are shown with thin lines. Relative energies are given in eV for the singlet multiplicity and included in the SI (xlsx) for all multiplicities. Metal atoms are shown in blue/green, oxygen atoms are shown in red and the carbon atom is shown in grey.

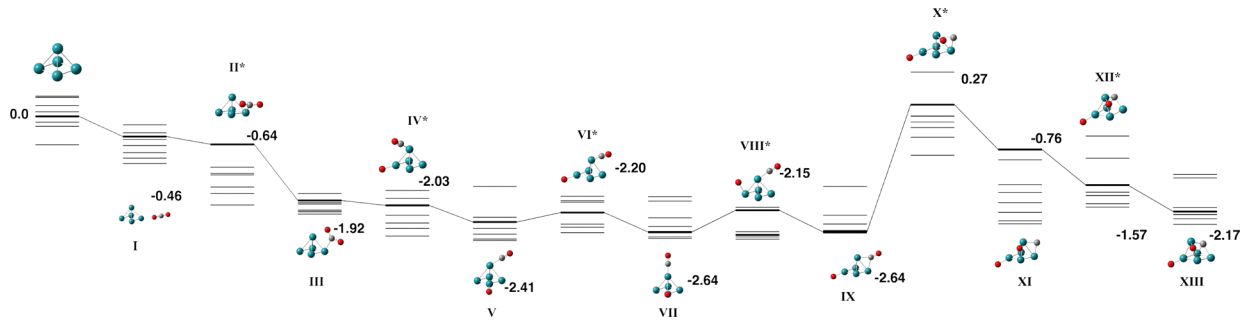


Fig. 5 Alternate reaction path on the $Ru_5$ + $CO_2$ potential energy surface. The singlet multiplicity is shown in bold and the triplet - 15-tet multiplicities are shown with thin lines. Relative energies are given in eV. Metal atoms are shown in blue/green, oxygen atoms are shown in red and the carbon atom is shown in grey.

higher in energy at all spin multplicities.[69] Nguyen and Pham[70] and Poulain and coworkers,[32] both employ a square pyramidal $Rh_5$ structure in their reactivity studies with $N_2O$.

Our initial search on the doublet surface, yielded a square pyramid ground state, but had a trigonal bipyramid structure only 0.12 eV higher in energy. Re-optimizing these structures at higher multiplicities (up to the 12-tet) showed that the sextet square pyramid was the lowest energy $Rh_5$ structure and that it is isoenergetic with the sextet and octet trigonal bipyramid structures. Therefore both square pyramid and trigonal bipyramid structures were considered for reaction with $CO_2$. In the reaction pathways below, pathways for the doublet – decet surfaces are presented as the 12-tet was higher in energy.

**3.4.1. Square pyramidal $Rh_5$.** Two pathways are shown for the square pyramid $Rh_5$ in Fig. 6 and 7 with geometric data in Table S4, it is possible to interconvert between them. The two pathways illustrate two "choices": Firstly, the capture species, when the $CO_2$ molecule first binds to the $Rh_5$ cluster, may employ either a base rhodium atom (Fig. 7) or an apex atom (Fig. 6). Either of these capture species leads to a bent $CO_2$ molecule bound to a Rh(apex)–Rh(base) bond, which is the lowest energy structure (Fig. 7-III and 6-III) at −1.61 eV. From this structure, the $CO_2$ molecule may break resulting in the CO molecule bound to the base rhodium atom (Fig. 7) with an energy of −1.06 eV, or leave the CO molecule bound to the apex rhodium atom (Fig. 6), where the barrier energy is −0.26 eV. This pathway leads to a structure (Fig. 6-VII), with CO $\mu^2$-bound to an Rh(apex)–Rh(base) bond and the dissociated oxygen atom $\mu^1$-bound to an adjacent Rh(base) atom, this structure is effectively isoenergetic with the bent $CO_2$ structure, Fig. 6-III. On either pathway, further dissociating the remaining CO molecule faces a high barrier, 1.20 or 1.92 eV above zero energy, indicating that $CO_2$ dissociation into three separate atoms is unlikely to occur on this cluster.

**3.4.2. Trigonal bipyramidal $Rh_5$.** A single pathway is presented for the reaction of trigonal bipyramid $Rh_5$ + $CO_2$ in Fig. 8 and Table S5. The features of the pathway are broadly similar to that of the square pyramidal pathways shown in Fig. 6 and 7. The $CO_2$ molecule approaches an apex rhodium atom, a bent $CO_2$ molecule lies across a Rh(apex)–Rh(equatorial) bond (Fig. 8-III), the first CO bond breaks leaving the CO molecule bound to an apex rhodium atom, leading to the lowest energy structure, Fig. 8-IX at −1.98 eV, where the oxygen atom is $\mu^2$-bound to a Rh(apex)–Rh(equatorial) bond and the CO molecule is $\mu^1$-bound to an apex rhodium atom. Breaking the second CO bond requires 1.10 eV above zero energy.

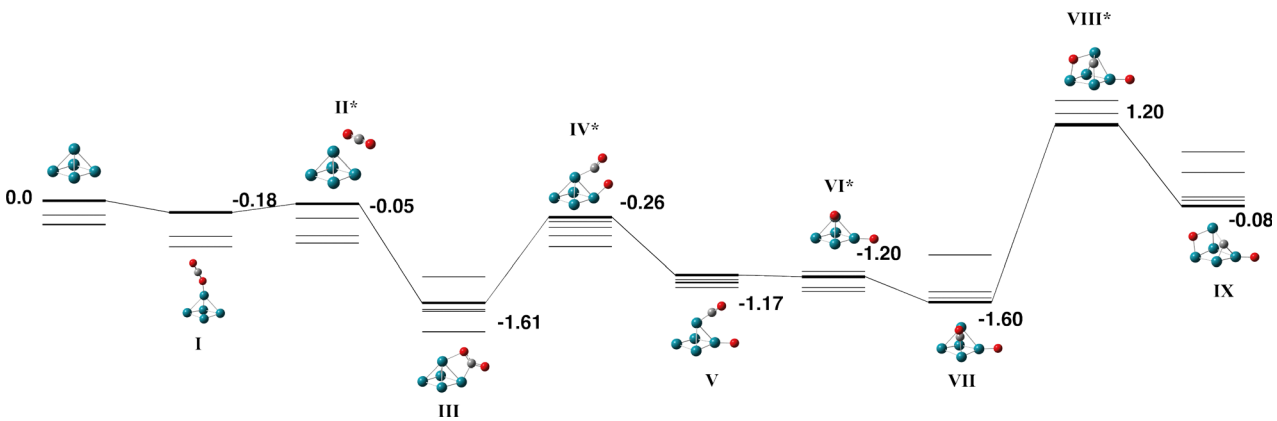


Fig. 6 Stationary points on the $Rh_5$ + $CO_2$ potential energy surface for the square pyramidal $Rh_5$ isomer. Doublet multiplicity is shown in bold and the quartet – decet multiplicities are shown with thin lines. Relative energies of doublet geometries are given in eV and included for all multiplicities in the SI (xlsx). Metal atoms are shown in blue/green, oxygen atoms are shown in red and the carbon atom is shown in grey.

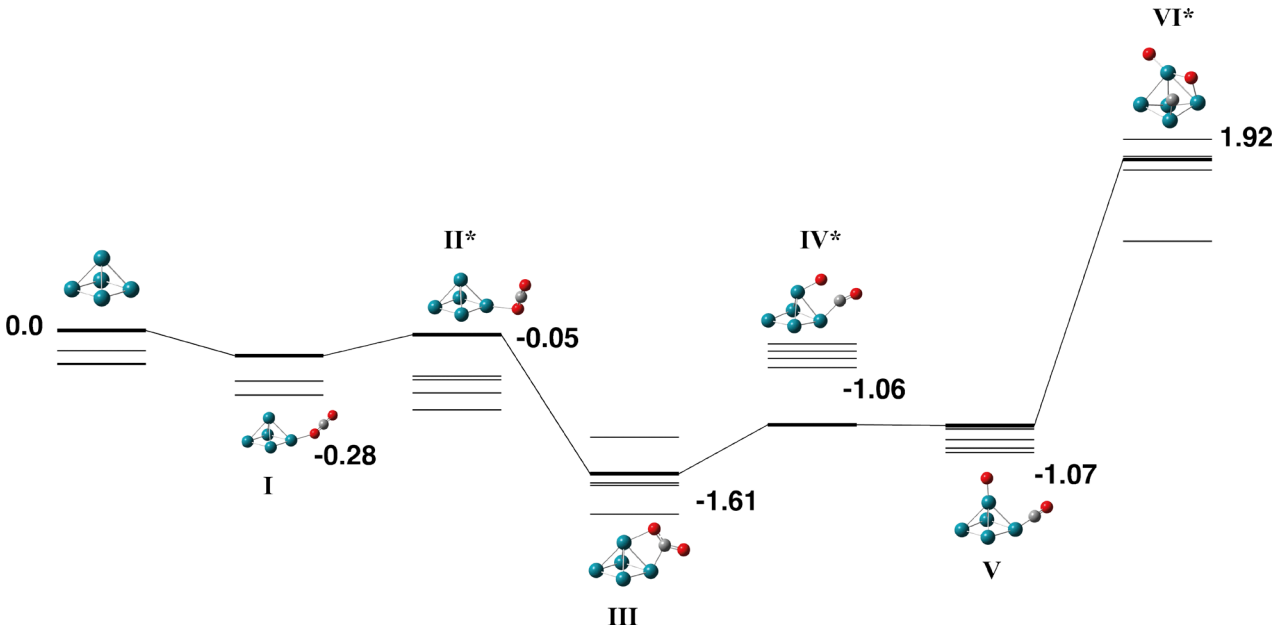


Fig. 7 Alternate pathway on the $Rh_5 + CO_2$ potential energy surface for the square pyramidal $Rh_5$ isomer. In this pathway, the first CO bond breaking in transition state VI leaves the CO molecule attached to the base Rh atom. The doublet multiplicity is shown in bold and the quartet – decet multiplicities are shown with thin lines. The final transition state leads to the same final structure as Fig. 6 as the CO breaks across the triangular $Rh_3$ face. Relative energies are given in eV. Metal atoms are shown in blue/green, oxygen atoms are shown in red and the carbon atom is shown in grey.

### 3.5. $Pd_5$

The $Pd_5$ cluster is an even-electron species and therefore we consider the singlet – septet multiplicities. Small Pd clusters have also been calculated by a variety of different methods over many years: Morokuma and coworkers predicted a $Pd_5$ ground state of a triplet trigonal bipyramid $Pd_5$ structure with $D_{3h}$ symmetry but noted a $C_{2v}$ trigonal bipyramid only 0.4 kcal $mol^{-1}$ higher in energy, and also a triplet $C_{4v}$ square pyramid only 2.3 kcal $mol^{-1}$ higher in energy.[71] Several other authors predict a triplet trigonal bipyramid structure.[72–76] Our search also identified a triplet trigonal bipyramid as the global minimum, and while we did not constrain symmetry, the structure has $C_{2v}$ symmetry. We did also identify the square pyramidal structure, the triplet was the lowest energy multiplicity for this structure and was 0.11 eV higher than the triplet trigonal bipyramid. While these two structures are sufficiently close in energy such that they are likely to coexist, we choose only the trigonal bipyramid to react with $CO_2$.

The $Pd_5 + CO_2$ reaction pathway is shown in Fig. 9 and Table S6, the quintet and septet pathways were high in energy and so only the singlet and triplet are shown. The capture species and adjacent transition state (structures Fig. 9-I and II) are shown for both an apex atom approach and an equatorial atom approach. Both approaches result in a bent $CO_2$ molecule weakly bound to the central Pd(apex)–Pd(equatorial) bond with a binding energy of −1.34 eV relative to the zero energy. This is the global minimum structure for the pathway, breaking the first of the two CO bonds requires +1.08 eV and the barrier to breaking the second CO bond is +4.45 eV.

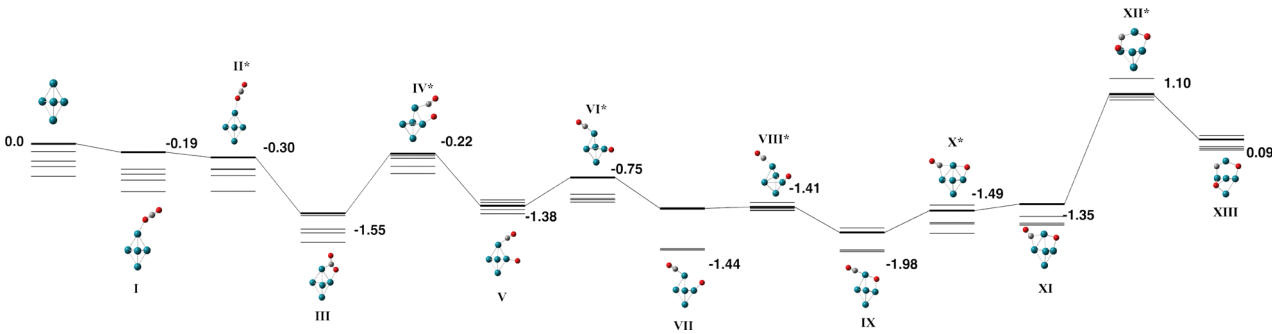


Fig. 8 Reaction pathway for trigonal bipyramidal $Rh_5 + CO_2$. The doublet multiplicity is shown in bold and the quartet – decet multiplicities are shown with thin lines. Relative energies shown are for the doublet surface and are given in eV, relative energies for all multiplicities are included in the SI (xlsx). Metal atoms are shown in blue/green, oxygen atoms are shown in red and the carbon atom is shown in grey.

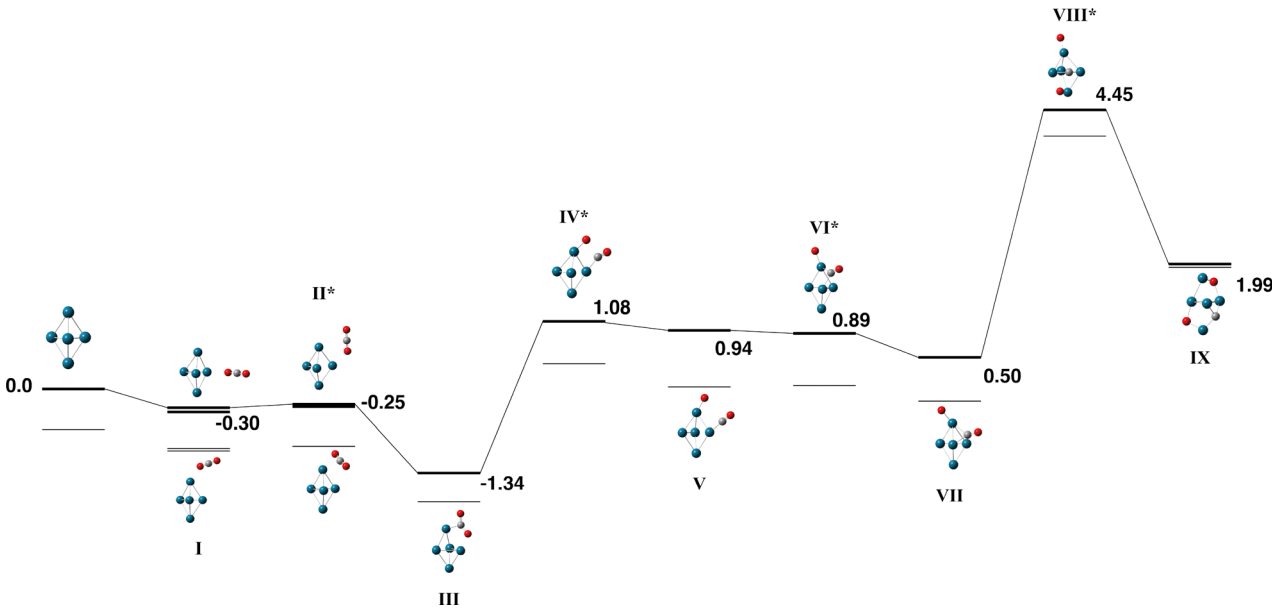


Fig. 9 Stationary points on the $Pd_5 + CO_2$ potential energy surface. The singlet multiplicity is shown in bold and the triplet multiplicity is shown with thin lines. Relative energies corresponding to singlet geometries are given in eV, all relative energies are included in SI (xlsx). Metal atoms are shown in blue/green, oxygen atoms are shown in red and the carbon atom is shown in grey.

### 3.6. $Pt_5$

The 5d transition metal, platinum was also studied due to its intense interest and frequent use as a catalyst. The $Pt_5$ cluster is studied at the singlet – septet multiplicities. A variety of structures have been obtained for the $Pt_5$ cluster with significant differences in predicted energetics and several authors debating whether the cluster is planar or three-dimensional.[77] Sumer and Jellinek identified several $Pt_5$ low-energy isomers, including a planar edge-capped square, trigonal bipyramid, edge-capped tetrahedron, square pyramid, planar trapezoidal and planar bowtie. On inclusion of spin–orbit effects, only the first three structures remained.[60] Kleinman and coworkers also studied the effect of spin–orbit coupling identifying the planar edge-capped square, followed by square pyramid, trigonal bipyramid, trapezoidal and bowtie structures.[78] Wang *et al.* identified a quintet trigonal bipyramid as their gas-phase global minimum.[79] Sebetci predicts a edge-capped tetrahedron global minimum, followed by a distorted rhombus, a trigonal bipyramid, a bowtie and trapezoidal structures.[80] Grönbeck and Andreoni noted that the class of density functional had a strong effect on the predicted isomer, with a planar edge-capped square favoured by BLYP whereas a distorted square pyramid was predicted by LSDA.[81] Singh *et al.* and Kumar and Kawazoe both predict the planar edge-capped square as the global minimum,[82,83] but Cao identified a square pyramidal structure as the basis of their reactivity study.[84] MRSDCI calculations of Majumdar *et al.* identified a distorted tetragonal pyramid.[85]

**3.6.1. Trigonal bipyramidal $Pt_5$.** In our search on the singlet surface, we identified bent trapezoidal, twisted bowtie, trigonal bipyramid and square pyramid structures all within 0.05 eV. The trigonal bipyramid and square pyramid structures were chosen to react with $CO_2$ and are shown in Fig. 10 and 11 respectively. Geometric data for both pathways is tabulated in Tables S7 and S8. Somewhat analogously to the $Pd_5 + CO_2$ reaction, the lowest energy $Pt_5CO_2$ structure at −1.67 eV has a bent $CO_2$ molecule bound to a Pt(apex)–Pt(equatorial) bond. This minimum could convert *via* a structure with $\mu^2$-bound CO and a $\mu^1$-bound oxygen atom (structure Fig. 10-V) (−0.77 eV) to a low-energy (−1.50 eV) structure (Fig. 10-VII) with the CO molecule $\mu^1$-bound to an equatorial platinum atom and the dissociated oxygen atom $\mu^1$-bound to an apex platinum atom. From that structure, dissociating the CO molecule has a barrier of +3.85 eV, and the product is also higher than zero energy by +2.67 eV. This is consistent with the IR-MPD + DFT study of Green *et al.*, who did not observe $CO_2$ frequencies in their $[Pt_5CO_2]^-$, but did observe a band at 1980 $cm^{-1}$, which they assigned to $\eta^1$-bound CO.[52]

**3.6.2. Square pyramidal $Pt_5$.** The pathway for the reaction of $CO_2$ to the square pyramidal isomer of $Pt_5$ is shown in Fig. 11 and Table S8. The $CO_2$ molecule approaches the apex platinum atom before twisting over a triangular face of the cluster (structure Fig. 11-III, −0.84 eV). Breaking the first CO bond requires +0.25 and +0.14 eV on the singlet and triplet surfaces, but is exothermic by −0.09 and −0.53 eV for the triplet and septet surfaces respectively. The lowest energy structure, Fig. 11-V, at −0.88 eV, has the CO molecule $\mu^2$-bound across a Pt(apex)–Pt(base) bond and the dissociated oxygen atom $\mu^1$-bound to a platinum atom on the base of the cluster. Attempting to continue the pathway search to break the second CO bond resulted in the $Pt_5$ cluster deforming to a trigonal bipyramid, applying constraints to the $Pt_5$ coordinates resulted in structures with multiple imaginary frequencies. The fluxional nature of small transition metal complexes is well known, and it is not unexpected that these two $Pt_5$ clusters may interconvert.

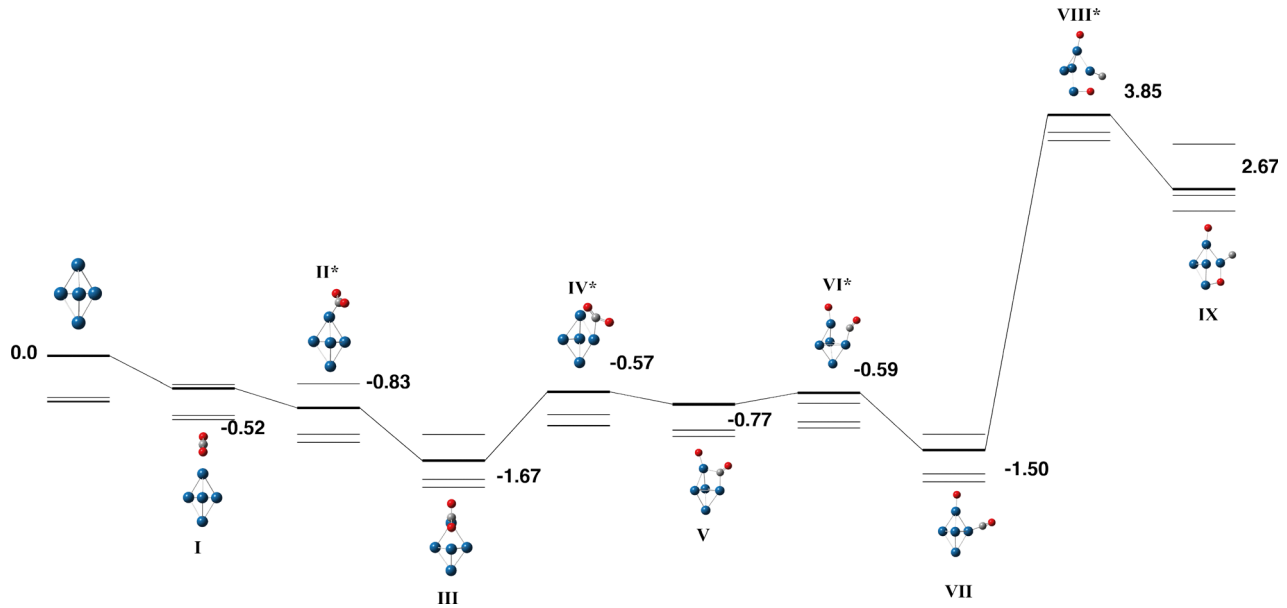


Fig. 10 Stationary points on the $Pt_5 + CO_2$ potential energy surface beginning with the trigonal bipyramidal $Pt_5$ isomer. The singlet multiplicity is shown in bold and the triplet – septet multiplicities are shown with thin lines. Relative energies for the singlet surface are given in eV, relative energies for all multiplicities are included in SI (xlsx). Metal atoms are shown in blue/green, oxygen atoms are shown in red and the carbon atom is shown in grey.

### 3.7. $Ag_5$

The $Ag_5$ cluster is an odd-electron species and we consider the doublet – octet multiplicities. Atolabi *et al.* conducted one of several studies into the gas-phase $Ag_5$ structure and predicted that the doublet planar trapezoidal structure was 0.49 eV lower in energy than the doublet trigonal bipyramid structure.[86] The B3PW91 calculations of Hisayoshi and coworkers predicted a similar energy difference of 0.53 eV.[87] Fournier,[88] Wang and coworkers,[89] and Koutecký and coworkers all predict a $C_{2v}$ doublet trapezoidal structure.[90] Fazli and coworkers also employed a trapezoidal $Ag_5$ cluster in their DFT study. Recent synthetic advances have produced a ligand-free trigonal bipyramid $Ag_5$ cluster,[91] which has been tested as an anti-tumour agent.[92] The same cluster was employed by Atolaibi *et al.* in their DFT-study with $CO_2$, $CH_4$, and $H_2O$ molecules. While these authors considered the trapezoidal $Ag_5$ isomer for reaction with $CH_4$ and indicated that the trapezoidal isomer was more stable, they only calculated the trigonal bipyramid for their calculations with $CO_2$, showing weak interaction of the $CO_2$ molecule with both the apex and equatorial silver atoms.[93]

The trapezoidal $Ag_5$ structure was chosen as the basis for the reaction path search, and the resulting pathway for the reaction of $Ag_5 + CO_2$ is shown in Fig. 12 with geometric data tabulated in Table S9. The doublet surface only is presented as all higher

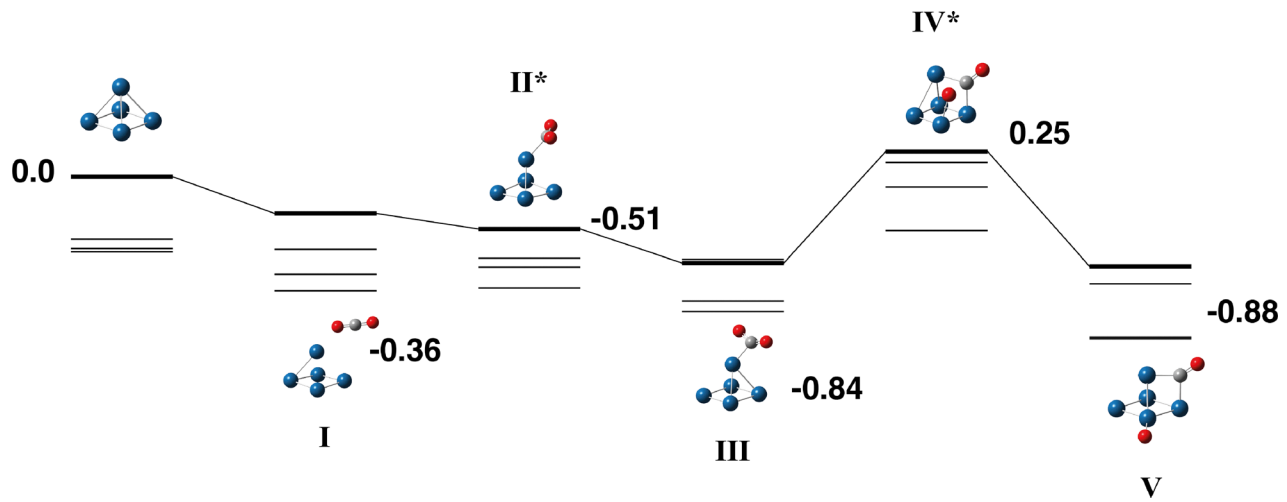


Fig. 11 Stationary points on the $Pt_5 + CO_2$ potential energy surface for the square pyramidal $Pt_5$ isomer. The singlet multiplicity is shown in bold and the triplet – septet multiplicities are shown with thin lines. Singlet relative energies are given in eV, other multiplicities are included in SI (xlsx). Metal atoms are shown in blue/green, oxygen atoms are shown in red and the carbon atom is shown in grey.

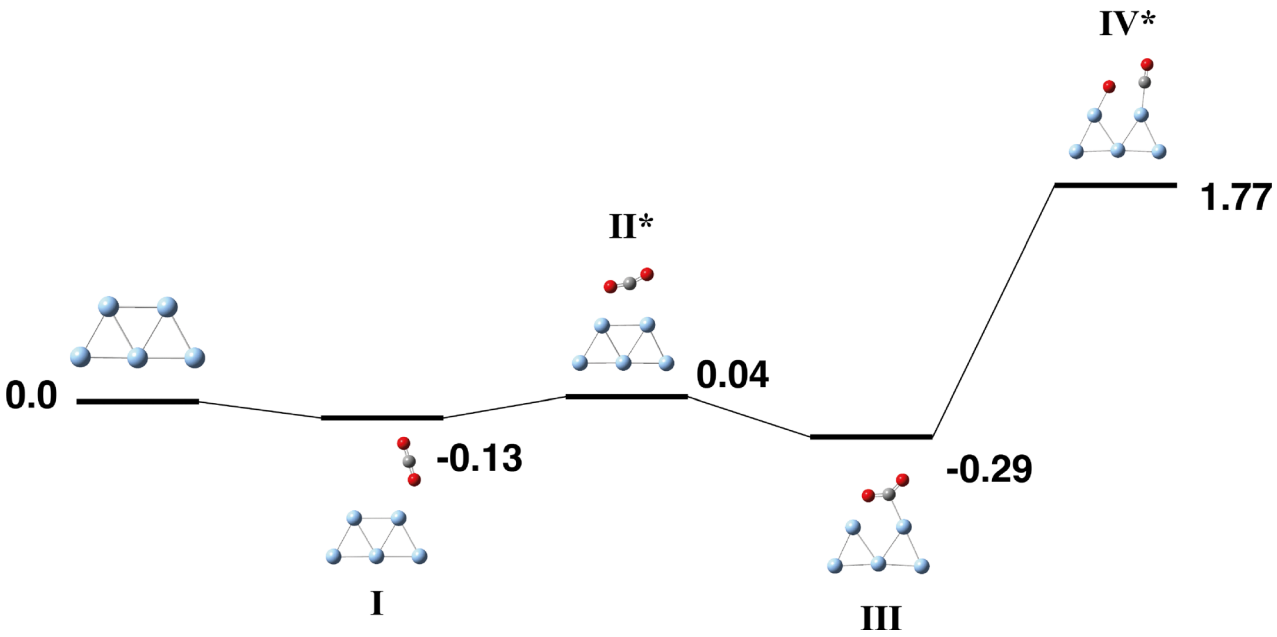


Fig. 12 Reaction pathway for the $Ag_5$ + $CO_2$ doublet potential energy surface. Other multiplicities are high in energy and are not shown. Relative energies are given in eV, and are included for higher multiplicities in the SI (xlsx). Metal atoms are shown in blue/green, oxygen atoms are shown in red and the carbon atom is shown in grey.

multiplicities were more than 1 eV higher in energy. $CO_2$ interacts only very weakly with the $Ag_5$ cluster, the capture species has the $CO_2$ molecule interacting with one of the atoms on the short edge of the trapezoid and is only −0.13 eV below zero energy. Only one other structure, Fig. 12-III was below zero energy, with an energy of −0.29 eV. Attempting to break the first $CO_2$ bond requires +1.77 eV. Searches were made for structures with the $CO_2$ molecule dissociated (*e.g.* CO + O, C + 2(O)), and an IRC was started from the transition state Fig. 12-IV, but in all these calculations the $Ag_5$ cluster did not remain intact and therefore we did not continue the reaction path.

### 3.8. Periodic trends

A previous computational study on the reaction of carbon monoxide, CO, with second-row transition metal timers showed that capture species were very similar in energy across the periodic table, with the exception of silver clusters, which bound CO only weakly.[31] This was observed similarly here for the $M_5$ clusters with $CO_2$, and is shown in Fig. 13. The consistent energy of the capture species can be rationalized in both cases that the capture species is defined as the first interaction of the two species and represents physisorption, where the chemical/electronic structure of the two species is barely perturbed. This is also consistent with the axial and equatorial, or apex and base capture species having similar interaction energies, where both were identified for the one $M_5$ cluster.

In the previous study of the interaction of $M_3$ + CO, there were only two other species of interest, the associative and dissociatively bound species.[31] In the case of $CO_2$ as a reactant, there are now three species of interest: the lowest energy bound OCO, the lowest energy O + CO and the lowest energy fully dissociated 2(O) + C structure. The energies of the associatively bound OCO species are relatively similar across the periodic

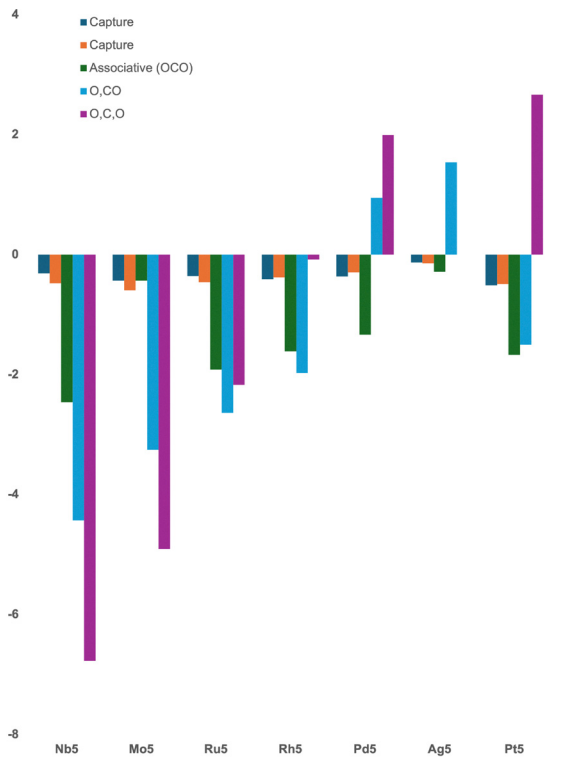


Fig. 13 Plot of the relative energies of capture, lowest energy associative (OCO), lowest energy partly dissociated (O,CO) and fully dissociative (O,C,O) structures of $M_5$ metal clusters in the lowest possible multiplicity.

table, ranging from −2.463 eV ($Nb_5$) to −1.340 eV ($Pd_5$), the two exceptions were $Ag_5$, which binds weakly, with a $Ag_5\cdots OCO$ binding energy of only −0.289 eV, and $Mo_5$, where $CO_2$ molecule dissociates *via* interaction with the axial atom of the cluster only. In structure Fig. 3-II, the C···O distance is 1.80 Å and the $\theta_{OCO}$ angle is 122°. The lowest energy associative structure for $Mo_5CO_2$ is therefore the capture species.

Similar trends are observed for the energies of the partly dissociative (O + CO) and fully dissociative (2(O) + C) structures. Both energies rise moving left to right across the second row of transition metals (Nb–Ag). The $M_5O$ + CO energies become disfavourable (positive) for $Pd_5$, while the fully dissociated structures are disfavoured to the right of $Rh_5$ inclusive. The lone third row pentamer in this study, $Pt_5$, favourably dissociates $CO_2$ to CO + O, but the fully dissociative structure is disfavoured with respect to the zero energy, $Pt_5$ + $CO_2$.

Table 1 shows the calculated vibrational frequencies of $CO_2$ in the capture species for each $M_5$ cluster. The two bending frequencies, now non-degenerate, are red-shifted by ≈60 $cm^{-1}$, but no trend was observed for this reduction. The frequencies of the symmetric and asymmetric $CO_2$ stretches do not change significantly on interaction with the $M_5$ cluster. To attempt a diagnostic for the fate of $CO_2$, the energy of the $CO_2$ $\pi_u$ orbital and the $\Delta E$, with respect to the calculated value for free $CO_2$ (−0.03280 a.u.) is also shown in Table 1. For $Nb_5$ and $Mo_5$, a strong reduction in the orbital energy of ≈0.05 a.u. is observed. Both of these clusters dissociate $CO_2$ fully. All other $M_5$ clusters lowered the $CO_2$ $\pi_u$ orbital energy by ≈0.02 a.u. and no distinction between clusters that possess a fully intact $CO_2$ in their minimum energy structure *vs.* clusters that partly dissociate $CO_2$ to O + CO was observed. Nevertheless, the orbital energy does indicate those clusters that fully dissociate $CO_2$ into atoms.

Table 2 shows the Hirshfeld charges on $CO_2$ molecule in the capture species and the first transition state for each of the reaction pathways. The q($CO_2$) for the physisorbed capture species, as in the previously presented $M_4$ clusters,[39] is consistent and positive (≈0.1) for all $M_5$ clusters, except $Ru_5$ with $CO_2$ bound to the apex atom, suggesting that this species is actually a chemisorbed species. Considering the charge transfer observed in the first transition state, the same diagnostic holds for $M_5$ clusters also as the $M_4$ clusters; For the left-most three clusters, full $CO_2$ dissociation is thermodynamically possible, though for $Ru_5$, this would require surmounting a +0.27 eV barrier on the singlet surface, but a below zero energy barrier on higher multiplicity surfaces (see SI spreadsheet for details) having $q(CO_2) < -0.35\ e^-$. Right-most clusters, $Pd_5$ and $Ag_5$, do not dissociate either $CO_2$ bond and have low back-donation to $CO_2$, $< 0.2e^-$, and clusters that likely activate $CO_2$ without fully dissociating it, $Rh_4$, $Pt_4$, have intermediate $q(CO_2)$ values.

Table 2 Hirshfeld charge on $CO_2$ in capture species and first transition state for $M_5CO_2$ reaction pathways

| System | Capture species $q(CO_2)$ | TS 1 $q(CO_2)$ |
|---|---|---|
| $Nb_5$ | 0.142 | −0.418 |
| $Mo_5$ | 0.118 | −0.494 |
| $Ru_5$ apex | −0.381 | −0.3747 |
| $Ru_5$ base | 0.098 | −0.434 |
| $Rh_5$ sq. py. | 0.094 | −0.336 |
| $Rh_5$ tri. bipy. | 0.106 | −0.314 |
| $Pd_5$ a | 0.086 | 0.037 |
| $Pd_5$ b | 0.088 | 0.008 |
| $Ag_5$ | 0.043 | −0.112 |
| $Pt_5$ tri. bipy. | 0.121 | −0.247 |
| $Pt_5$ sq. py. | 0.095 | −0.332 |

Fig. 14 shows the barrier heights (transition state energies) for two key transition states in each pathway, corresponding to the breaking of the first and second CO bond. The trends seen are broadly similar to the equivalent $M_4$ clusters.[39] The left-right divide previously seen for both barriers between Ru/Rh, is slightly less clear for the $M_5$ clusters, with both $Ru_5$ and $Rh_5$ being likely to break the first CO bond, but not the second. The softer barriers for $Pt_5$ compared to $Pd_5$ also suggest that the first CO bond would break on this cluster, leading to O + CO products on the cluster surface in this case also. Han and coworkers studied a range of mono and bimetallic metal surfaces and made similar conclusions, that activation energies for $CO_2$ dissociation increase left to right across the periodic table, with Au, Ag, and Pd based alloys having $CO_2$ dissociation barriers >1.50 eV.[18]

Table 1 $CO_2$ vibrational frequencies ($\nu_{CO_2}$), key orbital energies and adsorption and interaction energies for $M_5CO_2$ capture species. Absolute energy of the $CO_2$ $\pi_u$ orbital is −0.893 eV (−0.03280 a.u)

| System | Bend 1 | Bend 2 | Symm stretch | Asym stretch | $E(M_{5,HOMO})$ | $E(M_{5,LUMO})$ | $E(\pi_u)$ | $\Delta E(\pi_u)$ | $E_{ads}$ | $E_{int}$ |
|---|---|---|---|---|---|---|---|---|---|---|
| | | | ($cm^{-1}$) | | | | (eV) | | | |
| $CO_2$ | 622 | 622 | 1283 | 2319 | | | −0.893 | 0.0 | | |
| $Nb_5$ | 554 | 577 | 1277 | 2341 | −4.332 | −2.730 | −2.351 | −1.458 | −0.483 | −0.484 |
| $Mo_5$ | 560 | 560 | 1279 | 2340 | −4.388 | −2.406 | −2.383 | −1.491 | −0.438 | −0.439 |
| $Ru_5$ apex | 521 | 557 | 1259 | 2323 | −5.655 | −2.817 | −1.394 | −0.502 | −0.361 | −0.370 |
| $Ru_5$ base | 462 | 585 | 1254 | 2326 | −4.637 | −2.808 | −1.476 | −0.583 | −0.462 | −0.466 |
| $Rh_5$ sq. py. | 546 | 571 | 1268 | 2325 | −4.970 | −3.471 | −1.455 | −0.563 | −0.282 | −0.452 |
| $Rh_5$ tri. bipy. | 528 | 571 | 1266 | 2328 | −5.028 | −3.226 | −1.446 | −0.554 | −0.188 | −0.499 |
| $Pd_5$ a | 583 | 587 | 1281 | 2326 | −5.304 | −4.239 | −1.512 | −0.620 | −0.301 | −0.346 |
| $Pd_5$ b | 581 | 587 | 1278 | 2325 | −5.373 | −4.252 | −1.609 | −0.716 | −0.368 | −0.369 |
| $Ag_5$ | 593 | 605 | 1281 | 2314 | −5.074 | −2.813 | −1.379 | −0.487 | −0.133 | −0.133 |
| $Pt_5$ tri. bipy. | 552 | 564 | 1277 | 2336 | −5.606 | −4.416 | −1.742 | −0.849 | −0.516 | −0.547 |
| $Pt_5$ sq. py. | 551 | 570 | 1261 | 2310 | −5.466 | −4.272 | −1.536 | −0.643 | −0.360 | −0.377 |


Fig. 14 Plot of the relative energies of barriers to dissociation of the first (blue) and second (orange) C···O bonds for $M_5CO_2$ reaction pathways on the lowest multiplicity (singlet or doublet) surface.

### 3.9. $M_4$ *vs.* $M_5$ clusters

Each reaction path presented here and for the equivalent $M_4$ clusters[39] may be distilled into a profile containing six species; the capture species, lowest energy $M_nCO_2$, $TS_{O\cdots CO}$, lowest energy $M_nO{\cdot}CO$, $TS_{C\cdots O}$ and lowest energy $M_nO{\cdot}C{\cdot}O$. These abbreviated reaction profiles are shown in Fig. S1–S7. Reactions on $M_5$ surfaces are typically more exothermic than the equivalent $M_4$ clusters. Excluding palladium, increasing the cluster size lowers the energy of the first barrier by $\approx$0.5 eV. This is consistent with the B3LYP results for $Zr_4$ and $Zr_5$ clusters computed by Ghanty and coworkers.[33] The height of the second barrier on adding the fifth metal atom is less consistent, lowering for Nb, Mo and Rh, but rising for the other metals. This is consistent with the left hand metals (Nb, Mo) dissociating $CO_2$ fully, right side metals (Pd, Ag, Pt) keeping $CO_2$ intact, and central metals (Ru, Rh) showing intermediate behaviour, which is therefore the most tunable by alteration of the cluster size.

## 4. Conclusions

We have explored the chemistry of $CO_2$ reaction on a series of $M_5$ transition metal clusters, by deriving reaction pathways using Density Functional Theory. $Rh_5$ and $Pt_5$ clusters had multiple competitive ground state geometries, and reaction paths were derived for each, noting that the trigonal bipyramid and square pyramidal geometries may interconvert.

Moving from left to right across the $M_5$ series, the energies of the capture species remained relatively constant as expected for the minimally interacting, physisorbed species. The energies of the lowest energy associatively-bound species with $CO_2$ fully intact also fell within a narrow range of −2.463 to −1.340 eV, generally rising from $Nb_5$ to $Ag_5$. The energetics of the partly (O + CO), and fully (O + C + O) dissociated species define the outcome of the reaction, with both rising strongly as one moves to the right of the periodic table. The partly dissociated species was found to be disfavoured with respect to the separated $M_5$ +$CO_2$ reactants for $Pd_5$, $Ag_5$ and $Pt_5$, while the fully dissociated species was disfavoured from $Rh_5$ and could not be located for $Ag_5$.

The energy of the $CO_2$ $\pi_u$ orbital was found to distinguish those structures that dissociate $CO_2$ fully ($Nb_5$ and $Mo_5$) from those that do not, but could not resolve clusters that partly dissociate $CO_2$ from those that leave $CO_2$ fully intact. The magnitude of charge transfer to the $CO_2$ fragment was found to be diagnostic with strong (>0.35e), weak (<0.2e) and intermediate values indicating full $CO_2$ dissociation, no dissociation, and activation respectively.

## Author contributions

NTTY, AN, YR, MR, IN: investigation, writing – original draft MAA: conceptualization of this study, methodology, writing – review and editing.

## Conflicts of interest

There are no conflicts to declare.

## Data availability

The data supporting this article have been included as part of the supplementary information (SI). Supplementary information: geometric parameters (pdf), structures (xyz) and energies, vibrational data (xlsx) for all pathways. See DOI: https://doi.org/10.1039/d5cp03418c.

## Acknowledgements

MAA is grateful for HPC time *via* the UK Materials and Molecular Modelling Hub *via* grant no. (EP/T022213).

## References

1 Y. Peng, J. Gao, Y. Zhang, J. Zhang, Q. Sun, Q. Du, Z. Tang and T. Zhang, *J. Energy Storage*, 2023, **58**, 106286.
2 X. Zhang, G. Liu, K.-H. Meiwes-Broer, G. Ganteför and K. Bowen, *Angew. Chem., Int. Ed.*, 2016, **55**, 9644–9647.
3 Z. Yang, C. Yue, W. Pang, H. Wang, X. Cong, S. Huang, J. Qi, J. Lv, M.-Y. Wang and X. Ma, *Chem. Eng. Sci.*, 2025, **317**, 122104.
4 M. Aresta, A. Dibenedetto and E. Quaranta, *Reaction Mechanisms in Carbon Dioxide Conversion*, Springer Berlin, Heidelberg, 2015, pp. 1–409.
5 T. Sakakura, J.-C. Choi and H. Yasuda, *Chem. Rev.*, 2007, **107**, 2365–2387.
6 J. M. Weber, *Int. Rev. Phys. Chem.*, 2014, **33**, 489–519.
7 M. C. Thompson, J. Ramsay and J. M. Weber, *J. Phys. Chem. A*, 2017, **121**, 7534–7542.
8 T. Foyen, Z. P. Alcorn, M. A. Ferno, A. Barrabino and T. Holt, *J. Pet. Sci. Eng.*, 2021, **196**, 107651.
9 X. Meng, L. Zhao, H. Guo, F. Sha, H. Shi, Z. Wu and J. Zhang, *Crystals*, 2019, **9**, 433.
10 R. Shahbaz and F. Bahadori, *Sustain. Chem. Pharm.*, 2025, **46**, 102099.

11 S. Kumari, M. Gusain, B. Y. Lamba and S. Kumar, *J. Mater. Chem. A*, 2025, **13**, 21352–21388.
12 J. Jang, E. P. Delmo, W. Chen, Z. Sun, D. H. C. Wan, Y. Liu, S. Zhu, Y. Wang, T. Li, H. Huang, J. Ge and M. Shao, *Carbon Energy*, 2025, e70019.
13 Y. Ren, H. Liu, F. Duan, S. Lu, X. Chen and M. Du, *J. Mater. Chem. A*, 2025, **13**, 24988.
14 B. Liu, J. A. Wang and D. Niu, *Carbon*, 2025, **243**, 120562.
15 Y.-X. Yu, *J. Colloid Interface Sci.*, 2025, **695**, 137799.
16 Á. Morales-Garca, A. Fernández-Fernández, F. Viñes and F. Illas, *J. Mater. Chem. A*, 2018, **6**, 3381–3385.
17 I. Persson, J. Halim, H. Lind, T. W. Hansen, J. B. Wagner, L.-Å. Näslund, V. Darakchieva, J. Palisaitis, J. Rosen and P. O. Å. Persson, *Adv. Mater.*, 2019, **31**, 1805472.
18 J. Ko, B.-K. Kim and J. W. Han, *J. Phys. Chem. C*, 2016, **120**, 3438–3447.
19 J. Yang, L. Sun, Z. He, W. Xu and J. Peng, *J. Mater. Sci.*, 2025, **60**, 4669–4686.
20 A. Jurado, K. Ibarra, Á. Morales-Garca, F. Viñes and F. Illas, *ChemPhysChem*, 2021, **22**, 2456–2463.
21 J. Li, J. Jia, X. Wang, X. Wang, J. Wang, C. Zhang, Y. Bai and X. Zhang, *Appl. Surf. Sci.*, 2025, **710**, 163887.
22 V. K. Ocampo-Restrepo, L. Zibordi-Besse and J. L. F. Da Silva, *J. Chem. Phys*, 2019, **151**, 214301.
23 J. M. Weber, *Int. Rev. Phys. Chem.*, 2014, **33**, 489–519.
24 H. Liu, L. An, P. Wang, C. Yu, J. Zhang, H. Shin, B. Peng, J. Li, M. Li, H. An, J. Yu, Y. Chen, P. Wang, K.-S. Lee, K. Lalit, Z. Liu, O. K. Farha, W. Huang, J. Z. Liu, L. Qi, K. Xie and E. H. Sargent, *Nat. Commun.*, 2025, **16**, 6185.
25 H. Schwarz, *Coord. Chem. Rev.*, 2017, **334**, 112–123.
26 M. Sievers and P. Armentrout, *Int. J. Mass Spec.*, 1998, **179–180**, 103–115.
27 A. M. Ricks, A. D. Brathwaite and M. A. Duncan, *J. Phys. Chem. A*, 2013, **117**, 11490–11498.
28 Z. Zhao, X. Kong, D. Yang, Q. Yuan, H. Xie, H. Fan, J. Zhao and L. Jiang, *J. Phys. Chem. A*, 2017, **121**, 3220–3226.
29 A. Iskra, A. S. Gentleman, A. Kartouzian, M. J. Kent, A. P. Sharp and S. R. Mackenzie, *J. Phys. Chem. A*, 2017, **121**, 133–140.
30 M. C. Thompson, L. G. Dodson and J. M. Weber, *J. Phys. Chem. A*, 2017, **121**, 4132–4138.
31 M. A. Addicoat, M. A. Buntine, B. Yates and G. F. Metha, *J. Comput. Chem.*, 2008, **29**, 1497–1506.
32 O. Olvera-Neria, R. Avilés, H. Francisco-Rodrguez, V. Bertin, R. Garca-Cruz, J. C. González-Torres and E. Poulain, *J. Mol. Mod.*, 2015, **21**, 80.
33 Megha, K. Mondal, A. Banerjee and T. K. Ghanty, *Phys. Chem. Chem. Phys.*, 2020, **22**, 16877–16886.
34 M. N. Collacique, V. K. Ocampo-Restrepo and J. L. F. Da Silva, *J. Chem. Phys*, 2022, **156**, 124106.
35 V. K. Ocampo-Restrepo, L. G. Verga and J. L. F. Da Silva, *J. Phys. Chem. C*, 2021, **125**, 26296–26306.
36 A. Yamada, K. Miyajima and F. Mafune, *Phys. Chem. Chem. Phys.*, 2012, **14**, 4188–4195.
37 P. C. D. Mendes, V. K. Ocampo-Restrepo and J. L. F. Da Silva, *Phys. Chem. Chem. Phys.*, 2020, **22**, 8998–9008.
38 A. E. Green, J. Justen, W. Schöllkopf, A. S. Gentleman, A. Fielicke and S. R. Mackenzie, *Angew. Chem., Int. Ed.*, 2018, **57**, 14822–14826.
39 S. Sherif, B. A. Velmurugan, N. Abbas, M. Shaikh and M. A. Addicoat, *Phys. Chem. Chem. Phys.*, 2025, **27**, 1.
40 M. A. Addicoat and G. F. Metha, *J. Comput. Chem.*, 2009, **30**, 57–64.
41 M. A. Addicoat, S. Fukuoka, A. J. Page and S. Irle, *J. Comput. Chem.*, 2013, **34**, 2591–2600.
42 A. D. Becke, *J. Chem. Phys*, 1993, **98**, 5648–5652.
43 P. J. Hay and W. R. Wadt, *J. Chem. Phys*, 1985, **82**, 270–283.
44 W. R. Wadt and P. J. Hay, *J. Chem. Phys*, 1985, **82**, 284–298.
45 P. J. Hay and W. R. Wadt, *J. Chem. Phys*, 1985, **82**, 299–310.
46 M. A. Addicoat, K. F. Lim and G. F. Metha, *J. Chem. Phys*, 2012, **137**, 034301.
47 J. Tao, J. P. Perdew, V. N. Staroverov and G. E. Scuseria, *Phys. Rev. Lett.*, 2003, **91**, 146401.
48 F. Weigend and R. Ahlrichs, *Phys. Chem. Chem. Phys.*, 2005, **7**, 3297–3305.
49 F. Weigend, *Phys. Chem. Chem. Phys.*, 2006, **8**, 1057–1065.
50 S. Grimme, S. Ehrlich and L. Goerigk, *J. Comput. Chem.*, 2011, **32**, 1456–1465.
51 E. M. Cunningham, A. S. Gentleman, P. W. Beardsmore and S. R. Mackenzie, *Phys. Chem. Chem. Phys.*, 2019, **21**, 13959–13967.
52 G. Meizyte, A. E. Green, A. S. Gentleman, S. Schaller, W. Schöllkopf, A. Fielicke and S. R. Mackenzie, *Phys. Chem. Chem. Phys.*, 2020, **22**, 18606–18613.
53 M. J. Frisch, G. W. Trucks, H. B. Schlegel, G. E. Scuseria, M. A. Robb, J. R. Cheeseman, G. Scalmani, V. Barone, G. A. Petersson, H. Nakatsuji, X. Li, M. Caricato, A. V. Marenich, J. Bloino, B. G. Janesko, R. Gomperts, B. Mennucci, H. P. Hratchian, J. V. Ortiz, A. F. Izmaylov, J. L. Sonnenberg, D. Williams-Young, F. Ding, F. Lipparini, F. Egidi, J. Goings, B. Peng, A. Petrone, T. Henderson, D. Ranasinghe, V. G. Zakrzewski, J. Gao, N. Rega, G. Zheng, W. Liang, M. Hada, M. Ehara, K. Toyota, R. Fukuda, J. Hasegawa, M. Ishida, T. Nakajima, Y. Honda, O. Kitao, H. Nakai, T. Vreven, K. Throssell, J. A. Montgomery Jr., J. E. Peralta, F. Ogliaro, M. J. Bearpark, J. J. Heyd, E. N. Brothers, K. N. Kudin, V. N. Staroverov, T. A. Keith, R. Kobayashi, J. Normand, K. Raghavachari, A. P. Rendell, J. C. Burant, S. S. Iyengar, J. Tomasi, M. Cossi, J. M. Millam, M. Klene, C. Adamo, R. Cammi, J. W. Ochterski, R. L. Martin, K. Morokuma, O. Farkas, J. B. Foresman and D. J. Fox, *Gaussian-16 Revision B.01*, 2016, Gaussian Inc., Wallingford CT.
54 L. Goodwin and D. R. Salahub, *Phys. Rev. A*, 1993, **47**, R774–R777.
55 J. Del Pla and R. Pis Diez, *J. Phys. Chem. C*, 2016, **120**, 22750–22755.
56 M. Ziane, F. Amitouche, S. Bouarab and A. Vega, *J. Nano. Res.*, 2017, **19**, 380.
57 Y.-H. Yin and J. Chen, *Comput. Theor. Chem.*, 2022, **1212**, 113720.

58 C. J. Pickard and R. J. Needs, *J. Phys. Cond. Mat.*, 2011, **23**, 053201.
59 Y. Wei, V. Veryazov and L. Kantorovich, *APL Mater.*, 2024, **12**, 031127.
60 A. Sumer and J. Jellinek, *J. Chem. Phys*, 2022, **157**, 034301.
61 L. Xue-Ling, *Chin. Phys. B*, 2010, **19**, 107103.
62 F. Aguilera-Granja, L. C. Balbás and A. Vega, *J. Phys. Chem. A*, 2009, **113**, 13483–13491.
63 Y.-C. Bae, H. Osanai, V. Kumar and Y. Kawazoe, *Mater. Trans.*, 2005, **46**, 159–162.
64 W. Zhang, H. Zhao and L. Wang, *J. Phys. Chem. B*, 2004, **108**, 2140–2147.
65 G.-X. Ge, H.-X. Yan, Q. Jing and Y.-H. Luo, *J. Cluster Sci.*, 2011, **22**, 473–489.
66 Y. Jinlong, F. Toigo and W. Kelin, *Phys. Rev. B*, 1994, **50**, 7915–7924.
67 M. A. Mora, M. A. Mora-Ramírez and M. F. Rubio-Arroyo, *Int. J. Quant. Chem.*, 2010, **110**, 2541–2547.
68 T. Futschek, M. Marsman and J. Hafner, *J. Phys. Condens. Matter*, 2005, **17**, 5927.
69 C.-H. Chien, E. Blaisten-Barojas and M. R. Pederson, *Phys. Rev. A*, 1998, **58**, 2196–2202.
70 H. M. T. Nguyen and N. T. T. Pham, *J. Phys. Chem. C*, 2014, **118**, 28562–28571.
71 J. Moc, D. G. Musaev and K. Morokuma, *J. Phys. Chem. A*, 2003, **107**, 4929–4939.
72 X. Xing, A. Hermann, X. Kuang, M. Ju, C. Lu, Y. Jin, X. Xia and G. Maroulis, *Sci. Rep.*, 2016, **6**, 19656.
73 V. Kumar and Y. Kawazoe, *Phys. Rev. B*, 2002, **66**, 144413.
74 M. Moseler, H. Häkkinen, R. N. Barnett and U. Landman, *Phys. Rev. Lett.*, 2001, **86**, 2545–2548.
75 B. Kalita and R. C. Deka, *J. Chem. Phys*, 2007, **127**, 244306.
76 Y. Mu, Y. Han, J. Wang, J.-G. Wan and G. Wang, *Phys. Rev. A: At., Mol., Opt. Phys.*, 2011, **84**, 053201.
77 L. Xiao and L. Wang, *J. Phys. Chem. A*, 2004, **108**, 8605–8614.
78 M. N. Huda, M. K. Niranjan, B. R. Sahu and L. Kleinman, *Phys. Rev. A*, 2006, **73**, 053201.
79 Y. Wang, B. Xiang, H.-Q. Yang and C.-W. Hu, *ACS Omega*, 2017, **2**, 3250–3259.
80 A. Sebetci, *Chem. Phys.*, 2006, **331**, 9–18.
81 H. Grönbeck and W. Andreoni, *Chem. Phys.*, 2000, **262**, 1–14.
82 N. B. Singh and U. Sarkar, *J. Mol. Mod.*, 2014, **20**, 2537.
83 V. Kumar and Y. Kawazoe, *Phys. Rev. B*, 2008, **77**, 205418.
84 P. Cao and H. Wang, *J. Phys. Conf. Ser.*, 2021, **1992**, 032151.
85 D. Majumdar, D. Dai and K. Balasubramanian, *J. Chem. Phys.*, 2000, **113**, 7928–7938.
86 M. Alotaibi, Q. Wu and C. Lambert, *Appl. Surf. Sci.*, 2023, **613**, 156054.
87 T. Yumura, M. Kumondai, Y. Kuroda, T. Wakasugi and H. Kobayashi, *RSC Adv.*, 2017, **7**, 4950–4959.
88 R. Fournier, *J. Chem. Phys.*, 2001, **115**, 2165–2177.
89 Y. Wang and X. G. Gong, *Eur Phys. J. D*, 2005, **34**, 19–22.
90 V. Bonačič-Koutecký, L. Češpiva, P. Fantucci and J. Koutecký, *J. Chem. Phys.*, 1993, **98**, 7981–7994.
91 I. R. Arias, D. Buceta, G. Barone, M. C. Giménez-López, H. Lozano, M. Lazzari and M. Arturo López-Quintela, *J. Colloid Interface Sci.*, 2022, **628**, 437–447.
92 V. Porto, D. Buceta, B. Domínguez, C. Carneiro, E. Borrajo, M. Fraile, N. Davila-Ferreira, I. R. Arias, J. M. Blanco, M. C. Blanco, J. M. Devida, L. J. Giovanetti, F. G. Requejo, J. C. Hernández-Garrido, J. J. Calvino, M. López-Haro, G. Barone, A. M. James, T. García-Caballero, D. M. González-Castaño, M. Treder, W. Huber, A. Vidal, M. P. Murphy, M. A. López-Quintela and F. Domínguez, *Adv. Func. Mater.*, 2022, **32**, 2113028.
93 M. Alotaibi, T. Alotaibi, M. Alshammari and A. K. Ismael, *Crystals*, 2023, **13**, 1691.